

Electronic Supporting Information

Enhanced permeation arising from dual transport pathways in hybrid polymer-MOF membranes

Norman C. Su^{a,b}, Daniel T. Sun^{b,c}, Christine M. Beavers^d, David K. Britt^b, Wendy L. Queen^{b,c}, and Jeffrey J. Urban*,^b

^aDepartment of Chemical and Biomolecular Engineering, University of California, Berkeley, California 94720, United States

^bThe Molecular Foundry, Lawrence Berkeley National Laboratory, Berkeley, California 94720, United States

^cInstitut des Sciences et Ingénierie Chimiques, École Polytechnique Fédérale de Lausanne (EPFL) CH 1051 Sion, Switzerland

^dAdvanced Light Source, Lawrence Berkeley National Laboratory, Berkeley, California 94720, United States

email: jjurban@lbl.gov

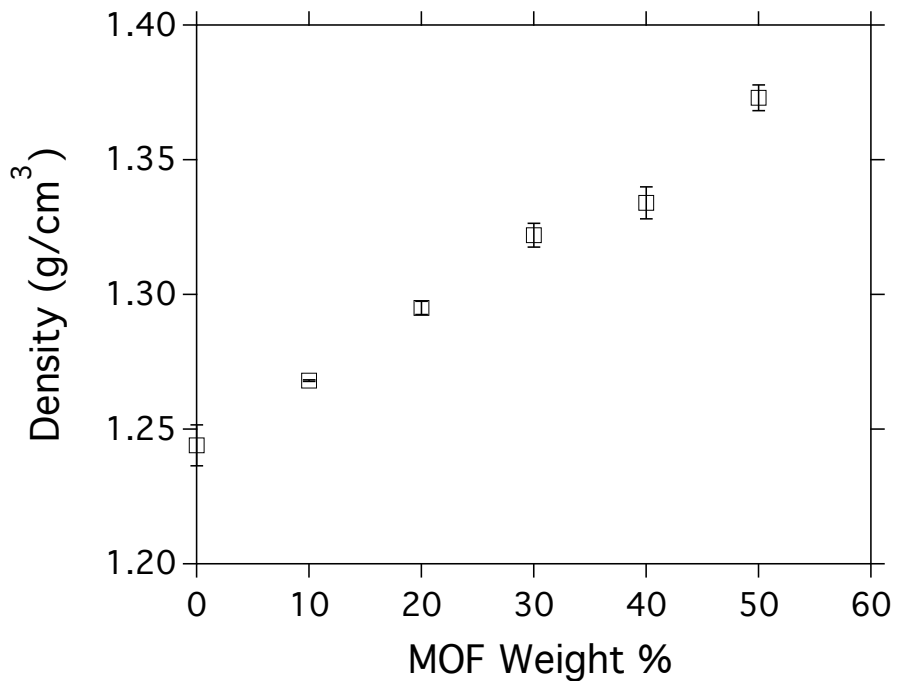


Fig. S1. Hydrostatic density measurement of UiO-66-NH_2 PSF hybrid membranes. Density follows a linear trend, indicating good interphase interaction.

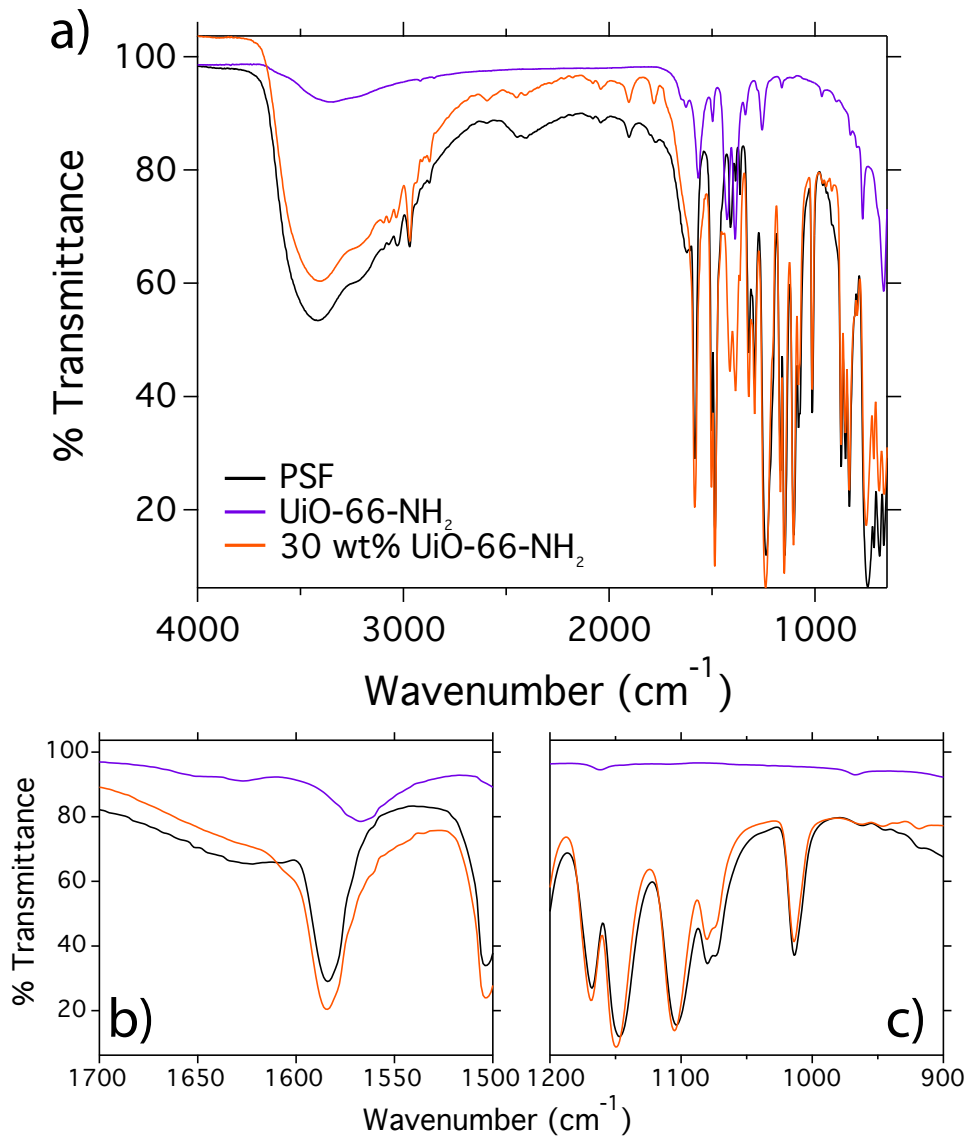


Fig. S2. a) FT-IR spectra of UiO-66-NH_2 , PSF, and 30 wt% $\text{UiO-66-NH}_2/\text{PSF}$. b) Primary amine peak of UiO-66-NH_2 at 1567 cm^{-1} becomes less apparent upon incorporation with PSF at 30 wt% indicating possible hydrogen-bonding interactions. c) Sulfonyl peak at 1150 and 1170 cm^{-1} does not shift with addition of UiO-66-NH_2

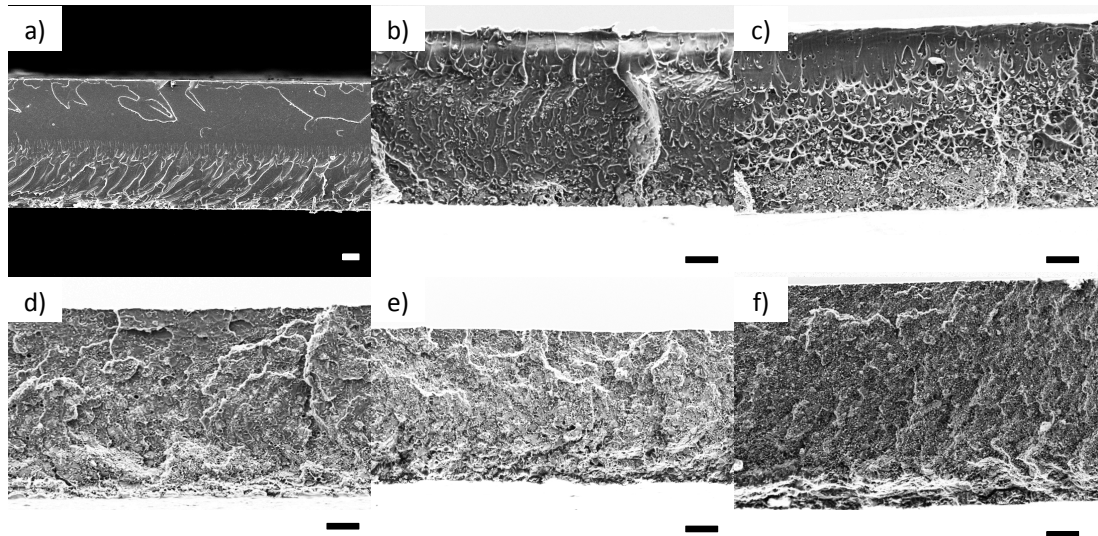


Fig. S3. Thickness of hybrid membranes. a) PSF, b) 10 wt% UiO-66-NH_2 , c) 20 wt% UiO-66-NH_2 , d) 30 wt% UiO-66-NH_2 , e) 40 wt% UiO-66-NH_2 , f) 50 wt% UiO-66-NH_2 . All scale bars represent 10 μm .

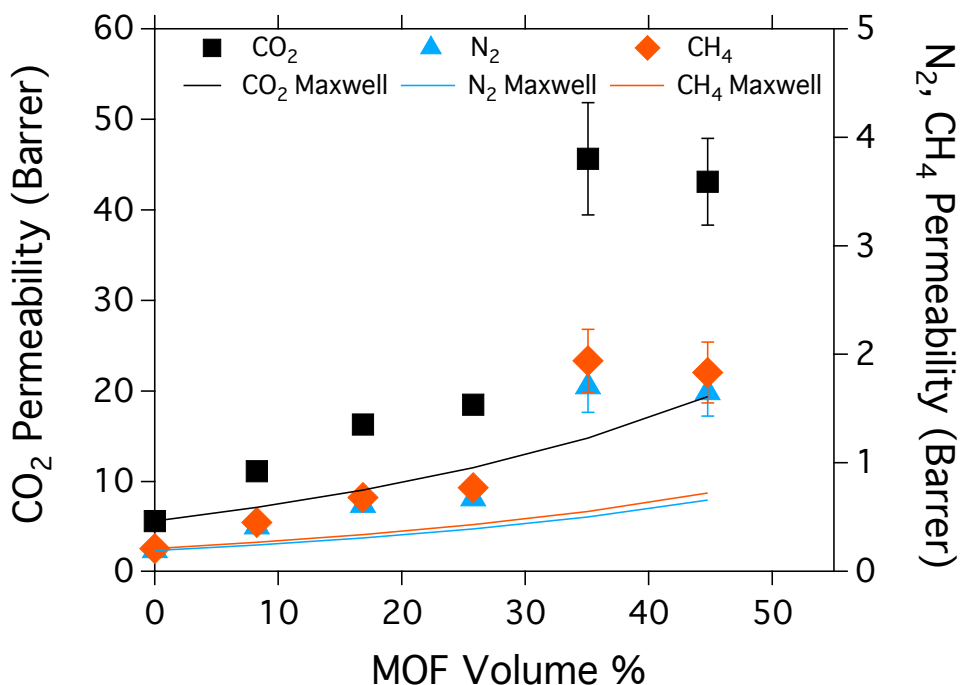


Fig. S4. Comparing Maxwell's predicted permeability with a spherical shape factor of $n = 1/3$ and $P_d = \infty$ to experimental permeability. Maxwell's permeability consistently underestimates permeability for CO_2 , N_2 , and CH_4 ; this breakdown in the predictive value of the model is accentuated for high MOF loadings

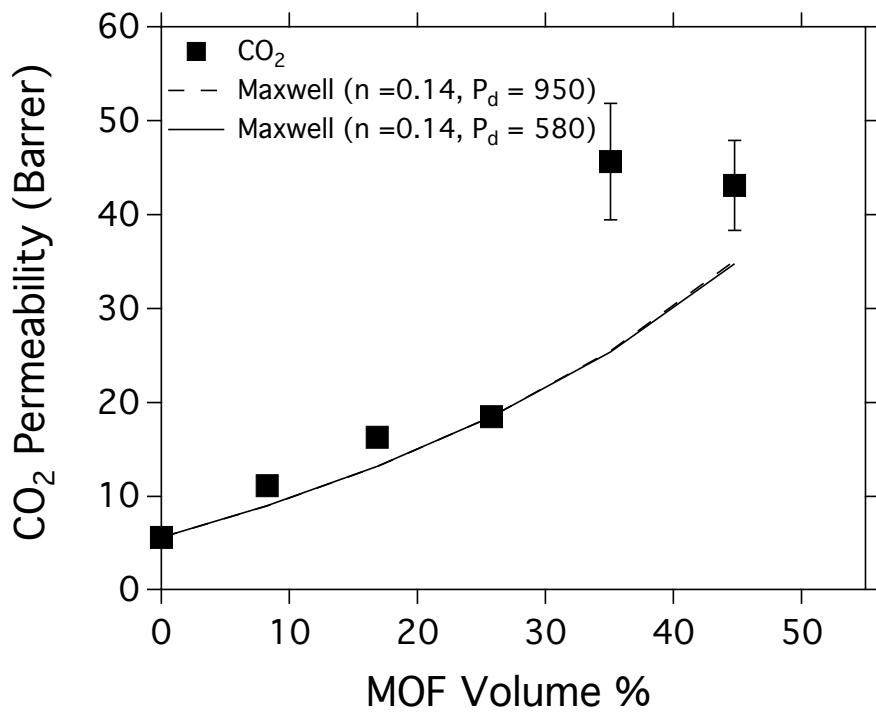


Fig. S5. Comparing Maxwell's permeability with an adjustable shape factor. *n* converges to 0.14. Permeability of UiO-66-NH₂ ranges from 500-1000 barrers. Maxwell permeability trends shown for 580 and 950 barrer. Excellent correlation with experimental permeability below 30 wt%.

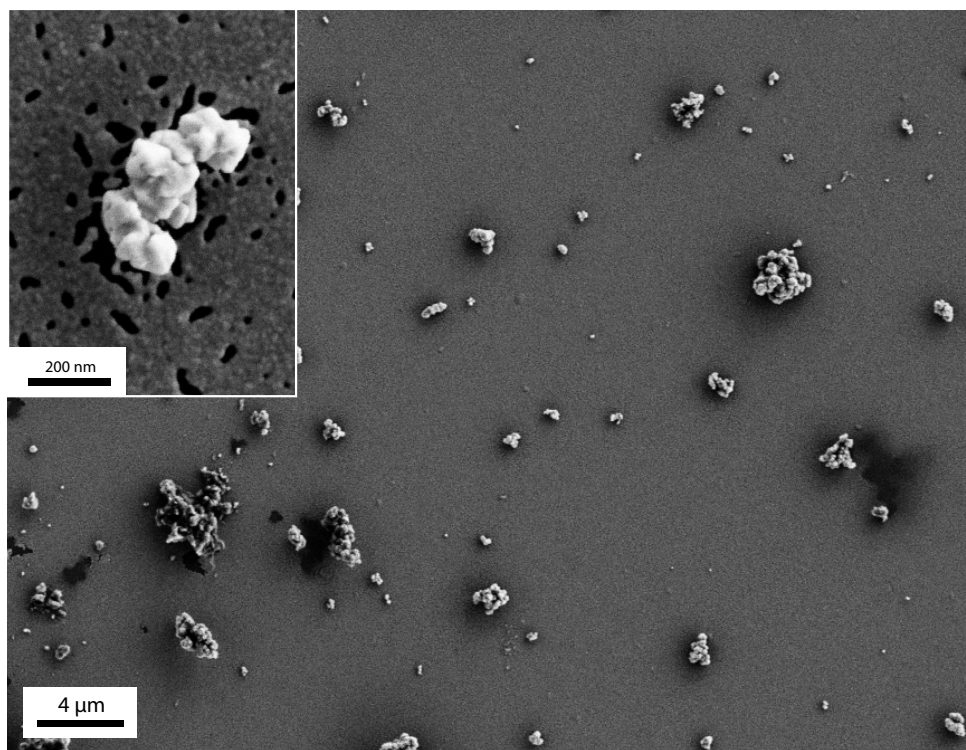


Fig. S6. SEM image of UiO-66-NH₂ nanoparticles. We observe partial aggregation of smaller domains of UiO-66-NH₂, which results in presence of elongated UiO-66-NH₂ ellipsoids (inset) consistent with percolation theory.

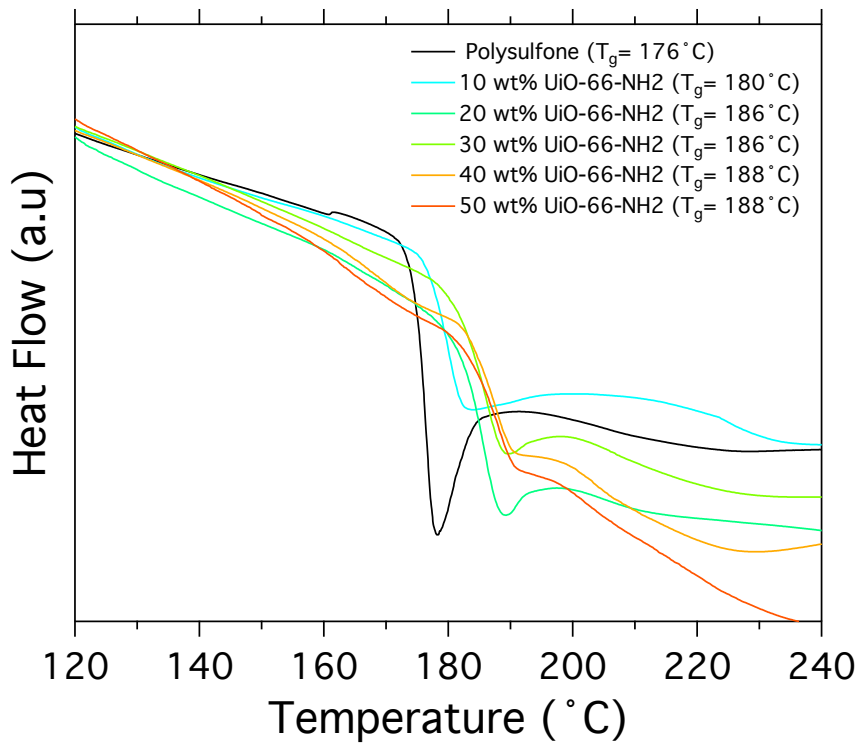


Fig. S7. DSC thermograms of UiO-66-NH_2 PSF hybrid membranes. Scan rate $20\text{ }^\circ\text{C}/\text{min}$. T_g increases with increasing MOF loading.

Table S1. CO₂, N₂, and CH₄ permeabilities in barrers for UiO-66-NH₂ at 3 bar and 35 °C

MOF Weight %	N ₂	CH ₄	CO ₂
0%	0.19 ± 0.011	0.21 ± 0.017	5.6 ± 0.32
10%	0.41 ± 0.012	0.45 ± 0.013	11 ± 0.32
20%	0.61 ± 0.032	0.68 ± 0.036	16 ± 0.86
30%	0.67 ± 0.017	0.77 ± 0.02	19 ± 0.47
40%	1.7 ± 0.024	1.9 ± 0.28	46 ± 6.2
50%	1.65 ± 0.022	1.8 ± 0.28	43 ± 4.8

Table S2. CO₂/CH₄ and CO₂/N₂ selectivities for UiO-66-NH₂ at 3 bar and 35 °C

MOF Weight %	CO ₂ /CH ₄	CO ₂ /N ₂
0%	27	30
10%	25	27
20%	24	27
30%	24	28
40%	24	27
50%	24	26

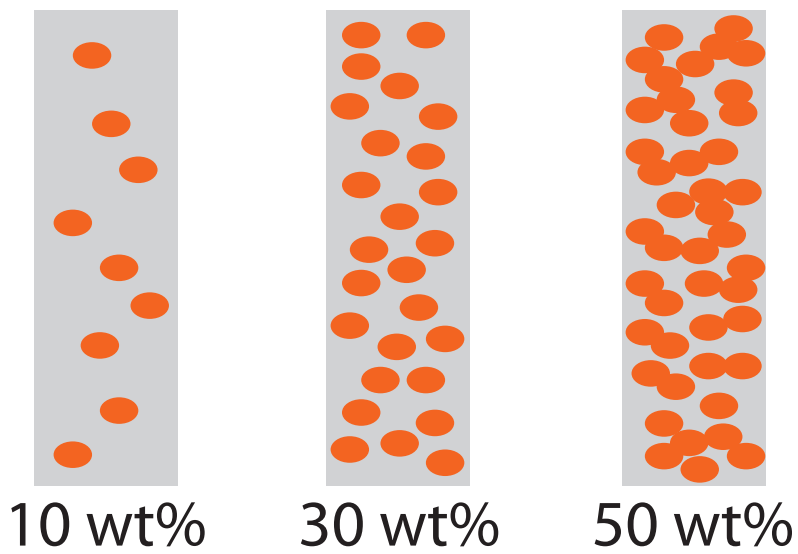


Fig. S8. Schematic of formation of percolative interconnected network of MOF crystals with ellipsoid geometry. Interconnected network of MOF crystals is formed when percolation threshold is reached.

Gas transport above the percolation threshold can be understood by the following equation:^{1,2}

$$P_{\text{Hybrid}} = P_{\text{cluster}}\phi_{\text{cluster}} + P_{\text{polymer}}(1 - \phi_{\text{cluster}})$$

where P_{Hybrid} is the permeability of the hybrid membrane, P_{cluster} is the permeability of the percolation cluster, ϕ_{cluster} is the volume fraction of the percolation cluster, and P_{polymer} is the permeability of the polymer. We were not able to quantify the volume fraction of the MOF that participated as a percolation cluster but we believe it to be only a small fraction of the total MOF available for transport.

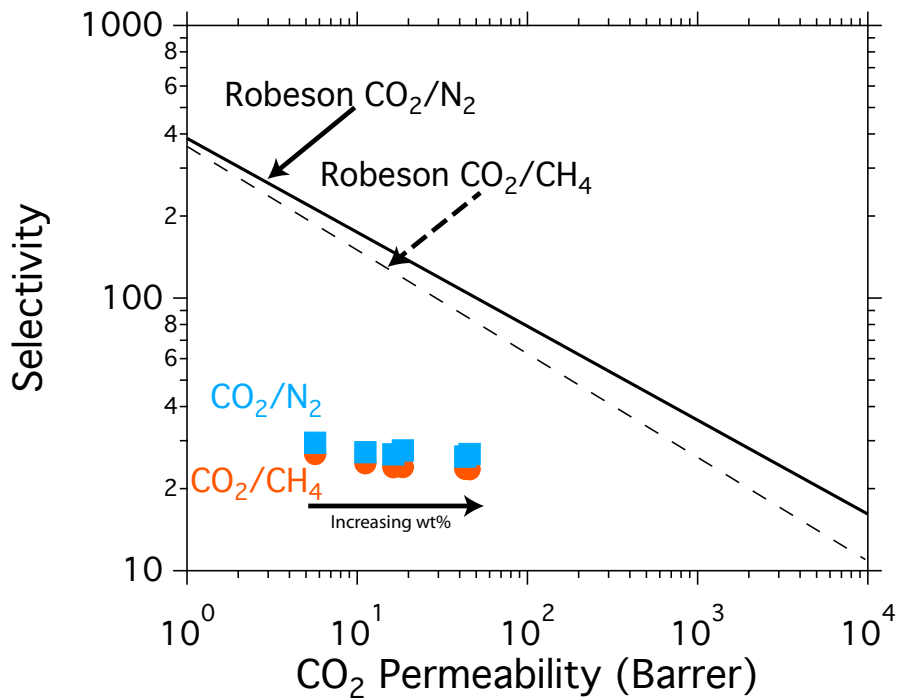


Fig. S9. Robeson upper bound plot of UiO-66-NH_2 PSF hybrid membranes for CO_2/N_2 and CO_2/CH_4 . In both cases, the addition of MOF moves the transport performance of the hybrid membrane closer to the upper bound line.

Table S3. Diffusivity, Solubility, and Gas Uptake Values for UiO-66-NH_2 membranes at 3 bar and 35 °C

MOF wt%	Diffusion*10 ⁸ (cm ² /s)			Solubility (cm ³ (STP)/(cm ³ atm))			Gas Uptake(cm ³ /(cm ³ atm))		
	N ₂	CH ₄	CO ₂	N ₂	CH ₄	CO ₂	N ₂	CH ₄	CO ₂
0%	0.72	0.18	1.1	0.20	0.90	4.0	0.63	2.8	12.5
10%	1	0.27	1.5	0.30	1.2	5.8	0.92	3.9	17.9
20%	1.3	0.42	1.9	0.35	1.2	6.4	1.1	3.8	19.8
30%	1.2	0.39	1.7	0.44	1.5	8.1	1.4	4.7	25.5
40%	1.5	0.7	3.1	0.92	2.3	11.6	2.8	7.2	36.0
50%	1.7	0.69	2.9	0.88	2.4	12.3	2.7	7.6	38.2

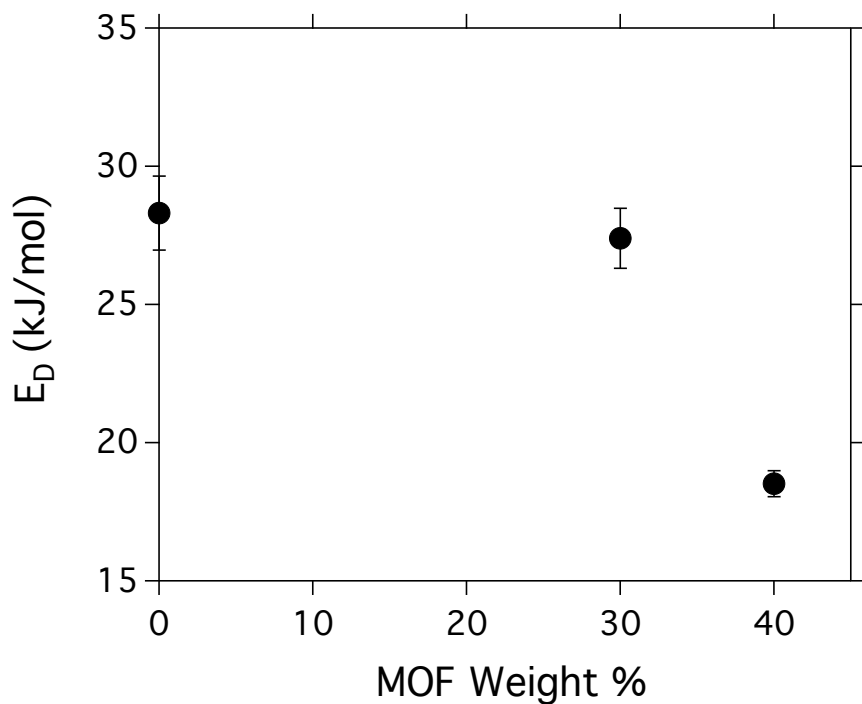


Fig. S10. CO_2 activation energy for diffusion, E_D as a function of MOF weight %. Under the percolation threshold (up to 30 wt% MOF), the activation energy shows no significant decrease. Over the percolation threshold (over 40 wt% MOF), E_D drops significantly due to the formation of dual transport pathways.

References:

1. Bakhtin, D., Eremin, Y. S., Grekhov, a. M. & Volkov, V. V. Gas Permeability of PVTMS/CNT Mixed Matrix Membranes. *Phys. Procedia* **72**, 166–170 (2015).
2. Eremin, Y. S. & Grekhov, a. M. Calculation of Percolating Clusters Characteristics in Mixed Matrix Membrane with CNT. *Phys. Procedia* **72**, 37–41 (2015).